nature materials

LETTERS

PUBLISHED ONLINE: 24 OCTOBER 2010 | DOI: 10.1038/NMAT2882

Direct observation and mapping of spin waves emitted by spin-torque nano-oscillators

Vladislav E. Demidov[1]*, Sergei Urazhdin[2] and Sergej O. Demokritov[1]

Dynamics induced by spin-transfer torque is a quickly developing topic in modern magnetism, which has initiated several new approaches to magnetic nanodevices[1–11]. It is now well established that a spin-polarized electric current injected into a ferromagnetic layer through a nanocontact exerts a torque on the magnetization, leading to microwave-frequency precession detectable through the magnetoresistance effect. This phenomenon provides a way for the realization of tunable nanometre-size microwave oscillators, the so-called spin-torque nano-oscillators[3,4,6] (STNOs). Present theories of STNOs are mainly based on pioneering works[12,13] predicting emission of spin waves due to the spin torque. Despite intense experimental studies, until now this spin-wave emission has not been observed. Here, we report the first experimental observation and two-dimensional mapping of spin waves emitted by STNOs. We demonstrate that the emission is strongly directional, and the direction of the spin-wave propagation is steerable by the magnetic field. The information about the emitted spin waves obtained in our measurements is of key importance for the understanding of the physics of STNOs, and for the implementation of coupling between individual oscillators mediated by spin waves[9–11,14]. Analysis shows that the observed directional emission is a general property inherent to any dynamical system with strongly anisotropic dispersion.

Spin-wave emission has been intensively theoretically analysed in recent years as an effective and compact mechanism for the enhancement of the oscillation coherence and output power by arrays of STNOs, as a result of their mutual synchronization[15–20]. Following this approach, experimental studies of two closely spaced STNOs demonstrated their mutual synchronization[9–11]. Although electrical measurements[11] indicate that interaction between STNOs mediated by spin waves plays an important role in synchronization, no direct study of the spin-wave emission by STNOs has been carried out so far. As the spin-wave emission by STNOs has not yet been observed, it remains unclear how the STNO arrays coupled by spin waves can be implemented in practice.

Experimental investigation of this effect requires a technique capable of detection and mapping of spin waves with a high spatial resolution. Here, we report the observation and mapping of spin waves emitted by STNOs by means of the recently developed micro-focus Brillouin light scattering (BLS) spectroscopy[21], which yields a signal directly proportional to the spin-wave intensity at a chosen location. Previous theoretical analyses[15–20] suggested that efficient spin-wave emission into a magnetic film surrounding a STNO is more likely if a strong magnetic field is applied perpendicular to the plane of the magnetic layers forming the oscillator, whereas in the more straightforward in-plane magnetization geometry the emission is suppressed owing to the strong nonlinear self-localization of spin waves. Our results show that spin-wave emission by STNOs can be achieved with the in-plane magnetization geometry, which is more amenable to applications because it does not require strong magnetic fields.

A schematic of our experiment is shown in Fig. 1a. The STNO device is formed by a nanocontact on an extended Permalloy (Py) film. The nanocontact is shaped as an elliptical nanopillar formed by the nanopattered polarizing $Co_{70}Fe_{30}$ layer and a Cu spacer. A d.c. current I flowing from the polarizer to the Py film induces local magnetization oscillations of the latter. The nanocontact is located within 200 nm from the edge of the top device electrode, enabling optical access to the Py film at larger distances. The spatially resolved detection of spin waves emitted by STNOs was carried out by micro-focus BLS spectroscopy[22]. The probing laser light was focused onto the surface of the Py film and scanned in-plane to record two-dimensional maps of the spin-wave intensity.

The oscillation characteristics of STNOs were determined from the microwave signals generated as a result of the magnetoresistance effect[4], as shown in Fig. 1b–d. The plots of the power spectral density illustrate the dependence of the oscillation frequency on the bias current I for three different angles φ between the in-plane bias magnetic field $H_0 = 900$ Oe and the easy axis of the nanostructured polarizer. The microwave generation starts at an onset current $I = 2.5$–3.5 mA that depends on φ. The dependence of the generation frequency on current above the onset is caused by the nonlinear frequency shift resulting from a combination of the demagnetizing effects in Py and the dipolar field of the structured $Co_{70}Fe_{30}$ polarizer[4]. For small φ, the nonlinear shift is strongly negative. It becomes less pronounced with increasing φ, and changes to positive at small I and $\varphi > 20°$. The region of positive nonlinear frequency shift is reduced at larger H_0, and eventually disappears for $H_0 > 1{,}200$ Oe, indicating that it originates from the dipolar field of the polarizer. The possibility to control the nonlinear behaviours by varying the angle φ makes the studied STNOs uniquely suited for the analysis of the effects of the nonlinearity on the spin-wave emission.

Figure 2 shows two-dimensional intensity maps of spin waves emitted by STNOs at $I = 5$ mA, measured for different in-plane directions of the bias field $H_0 = 900$ Oe. Several important conclusions can be made on the basis of the data in Fig. 2. First, STNOs with in-plane magnetization emit spin waves into the surrounding magnetic film. Second, the emission always occurs in the direction perpendicular to the in-plane field, regardless of its orientation, the generation frequency or the magnitude of the nonlinear frequency shift. We note that, although the sign of the nonlinear shift is expected to be important for the efficiency of spin-wave emission, the maps of Fig. 2a–d corresponding to significantly different nonlinear behaviours of the STNOs (see Fig. 1b–d) differ predominantly by the direction of emission, which rotates together with the field.

[1]Institute for Applied Physics and Center for Nonlinear Science, University of Muenster, Corrensstasse 2-4, 48149 Muenster, Germany, [2]Department of Physics, West Virginia University, Morgantown, West Virginia 26506, USA. *e-mail: demidov@uni-muenster.de.

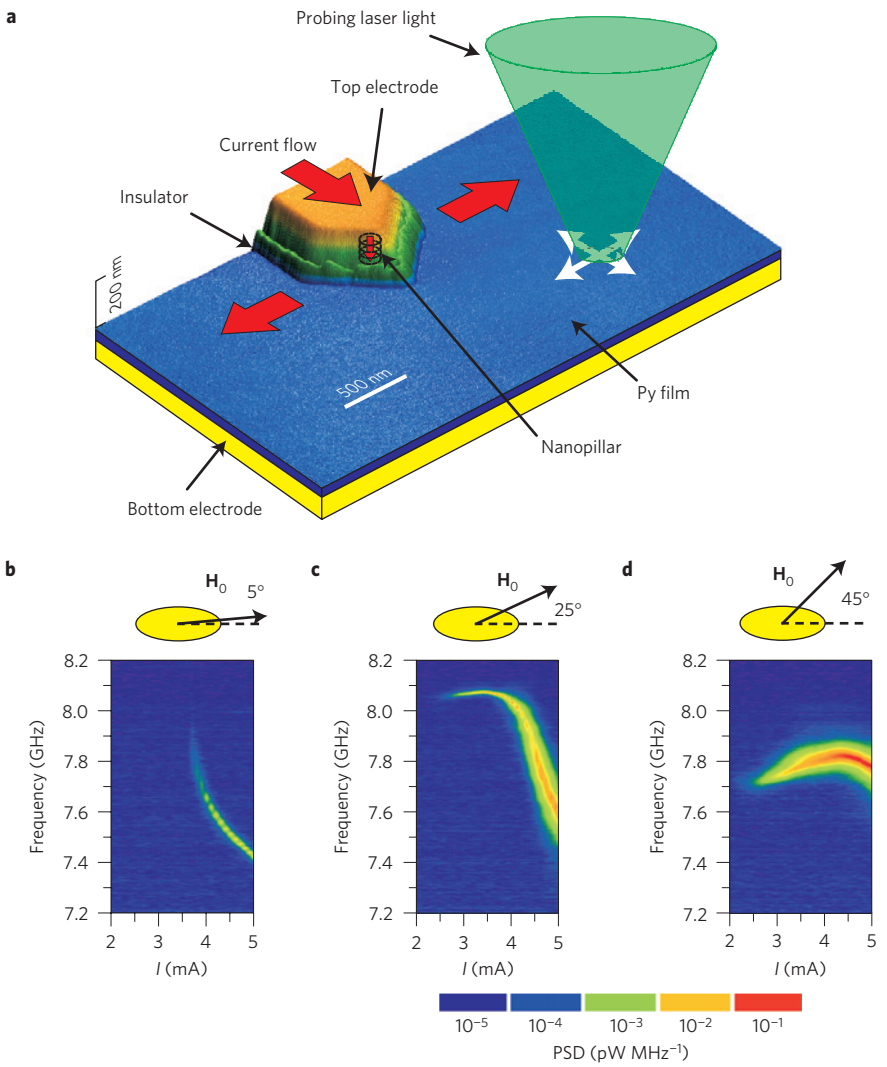

Figure 1 | Layout and characterization of the dynamical properties of STNOs. a, Schematic of the sample with an atomic force micrograph superimposed. The devices consist of an extended 6-nm-thick Permalloy free layer and an elliptical nanopillar formed by a 9-nm-thick $Co_{70}Fe_{30}$ polarizing layer and a 3-nm-thick Cu spacer. The nanopillar is located close to the edge of the top electrode enabling optical access to the free layer for BLS microscopy. Magnetic precession in the device is induced by d.c. current flowing from the polarizer to the free layer. The spatially resolved detection of spin waves is accomplished by focusing the probing laser light into a 250 nm spot, which is rastered over the surface of the Py film. **b**–**d**, Pseudo-colour logarithmic maps of the power spectral density (PSD) of the signal generated by the device as a result of the magnetoresistance effect at different angles φ between the in-plane bias magnetic field and the easy axis of the nanopillar, as labelled.

The observed features are reminiscent of the theoretical predictions of anisotropic emission made in ref. 18 on the basis of the interplay between the effects of the bias field and the Oersted field of the current. Indeed, we find evidence for the effects of the Oersted field in the noticeable asymmetry of the two oppositely directed emission lobes in Fig. 2d. The asymmetry inverted when H_0 was reversed, and decreased at larger H_0, indicating that it originates from the effect of the Oersted field of the current, which is aligned with H_0 in one direction of emission, and is opposed to it in the other direction. Nevertheless, the Oersted field cannot account for the observed directional emission perpendicular to the magnetic field, because in our measurements the directionality of emission did not depend on the magnitudes of the current or the magnetic bias field. We also emphasize that the observed emission patterns are qualitatively different from those observed for the linear spin-wave excitation by a microwave current[22], which can be attributed to the different selection rules for spin-wave emission due to the spin-torque phenomenon, as discussed below. The small spatial extent of the emitted spin waves suggests strong damping, probably due to a very short wavelength.

Figure 3 illustrates the spin-wave characteristics determined at the location of the maximum spin-wave intensity. Figure 3a–c shows the BLS spectra of the emitted spin waves for I increasing from 3 to 5 mA, together with the spectrum of the thermal spin waves. The spectra exhibit a small nonlinear frequency shift at $\varphi = 45°$, which increases as φ is reduced, in agreement with the electrical measurements shown in Fig. 1b–d. Figure 3d summarizes the dependencies of the frequency-integrated spin-wave intensity on the current I. As seen from these data, the intensity of the emitted spin waves increases linearly with current for the angle $\varphi = 45°$ characterized by a small nonlinear frequency shift. In contrast, the data for $\varphi = 25°$ and $\varphi = 5°$ exhibit a decrease of the spin-wave intensity starting from a certain value of current that decreases with decreasing φ. These findings are correlated with a larger nonlinear frequency shift, resulting in more significant reduction of the emission frequency below the ferromagnetic resonance. In contrast, magnetoresistance measurements (Fig. 1b–d) showed

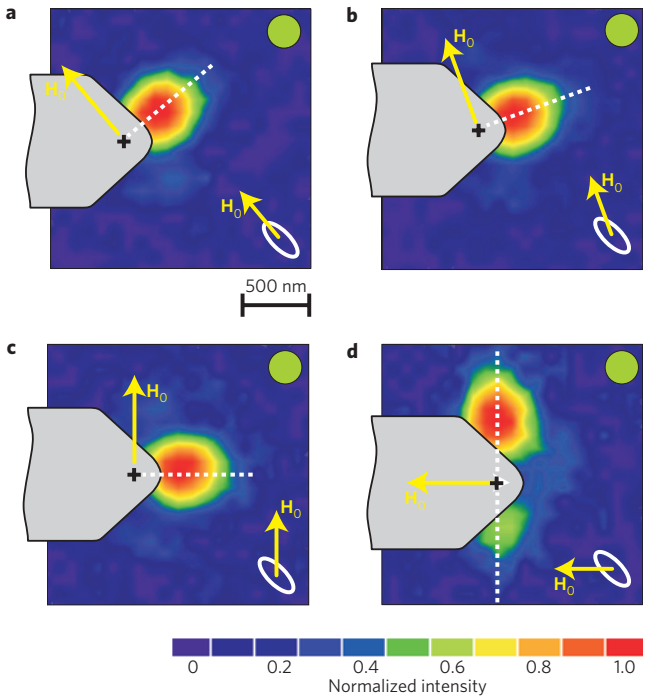

Figure 2 | Normalized colour-coded intensity maps of spin waves emitted by the STNOs. a–d, The maps with dimensions of 2 μm by 2 μm were recorded with a spatial step size of 100 nm at different angles φ between the in-plane bias magnetic field $H_0 = 900$ Oe and the easy axis of the elliptical nanopillar: $\varphi = 5°$ (**a**), $\varphi = 25°$ (**b**), $\varphi = 45°$ (**c**), $\varphi = -45°$ (**d**). The bias current is I = 5 mA. The schematic of the top electrode is superimposed on each map, with a cross indicating the location of the nanocontact. The intensity maps acquired at $I = 0$ were subtracted to eliminate the contribution from the thermal spin waves. The arrows show the direction of the static magnetic field, and the dashed lines indicate the direction of the spin-wave emission. The green circles on the maps indicate the size of the probing laser spot.

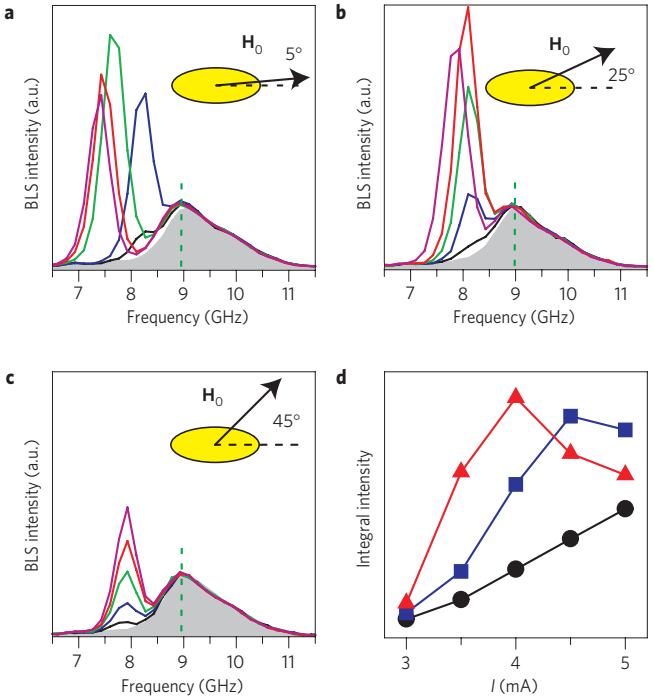

Figure 3 | Spectral characterization of the spin-wave emission. a–c, Dependence of BLS spectra on current for different in-plane directions of the bias field $H_0 = 900$ Oe, as indicated. The shadowed regions show the spectrum of the thermally excited spin waves determined by measurement at $I = 0$. The coloured lines show the spectra acquired at bias currents of 3.0 mA (black), 3.5 mA (blue), 4.0 mA (green), 4.5 mA (red) and 5.0 mA (pink). The dashed vertical lines mark the frequency of the ferromagnetic resonance. **d**, Dependencies of the integrated intensity of emitted spin waves on current for $\varphi = 5°$ (triangles), 25° (squares) and 45° (circles).

similar monotonic increases of generated power for all three configurations. Therefore, the decrease in the BLS intensity is associated with a decreased emission efficiency rather than a reduced amplitude of the oscillation in the nano-contact area.

We base our interpretation of the observed directional emission patterns on the analysis of the two-dimensional spin-wave spectrum[23] (Fig. 4a). As follows from Fig. 3, the STNO generation occurs near the minimum f_{min} of the spectrum. Expanding the spin-wave dispersion[24,25] into a Taylor series near the spectral minimum, and keeping the terms up to the second order in the wave vector, we obtain

$$f(k) = f_{min} + \frac{1}{2\pi}\left(\frac{\hbar(k_{\parallel} - k_{min})^2}{2m_{\parallel}} + \frac{\hbar k_{\perp}^2}{2m_{\perp}}\right) \qquad (1)$$

Here the direction of the wave vector $\mathbf{k} = (k_{\parallel}, k_{\perp})$ is defined with respect to the field $\mathbf{H}_0$, f_{min} and k_{min} label the point of the spectral minimum and $m_{\parallel} > m_{\perp}$ are the effective masses defined by the curvature of the dispersion at the minimum, $m_{\parallel,\perp} = (\hbar/2\pi)(\partial^2 f/\partial k_{\parallel,\perp}^2)^{-1}$. This definition is similar to the usual definition of effective masses of electrons in semiconductors[26]. We now demonstrate that the observed directionality of spin-wave emission is caused by the anisotropy of the effective masses.

First, we emphasize that the direction of the energy flow due to spin-wave propagation and, as a consequence, the geometry of the spin-wave pattern is determined by the direction of the group velocity, $\mathbf{V}_g = 2\pi\nabla f(k_{\parallel}, k_{\perp})$, which is not necessarily collinear with the wave vector. Let us assume that the STNO can be approximated as a point source generating spin waves at the frequency f_0 of the oscillation. In this case all spin waves satisfying $f(\mathbf{k}) = f_0$ (an ellipse in the momentum space, Fig. 4b) are excited with similar efficiency for all $k_{\parallel} < \pi/a_{\parallel}$ and $k_{\perp} < \pi/a_{\perp}$, where $a_{\parallel}$ and $a_{\perp}$ are the lateral dimensions of the STNO parallel and perpendicular to the field, respectively. Consequently, the intensity $\delta J_0(\theta)$ of spin waves emitted into an in-plane angle interval $\delta\theta$ is given simply by the phase volume $\delta\Gamma = (d\Gamma/d\theta)\delta\theta$, that is, the length of the segment of the $f(\mathbf{k}) = f_0$ contour corresponding to the direction of the group velocity $\mathbf{V}_g$ within this angular interval. As illustrated in Fig. 4b, the function $d\Gamma/d\theta$ is strongly anisotropic: for a given $\delta\theta$ the segment is significantly larger for $\theta = 90°$ (shown in yellow) than for $\theta = 0°$ (shown in cyan), resulting in a higher intensity of spin waves emitted perpendicular to $\mathbf{H}_0$.

In addition to the anisotropic emission, anisotropic damping also contributes to the angular dependence of spin-wave intensity $J(\theta)$ at a given distance from the STNO. In polar coordinates (θ, ξ), the effect of damping can be accounted for by $J(\xi, \theta) = J_0(\theta)\exp(-\xi/\lambda_r) = J_0(\theta)\exp(-\xi\omega_r/2|V_g(\theta)|)$, where $\lambda_r = 2V_g/\omega_r$ is the decay length determined by the spin-wave relaxation rate ω_r, which is considered to be independent of θ and the group velocity $V_g(\theta)$. According to equation (1), the group velocity reaches a maximum at $\theta = 90°$ and a minimum at $\theta = 0°$. As a consequence, the ratio of the intensities for these orthogonal directions increases exponentially with the distance from the STNO.

A calculation based on the above analysis of the angular dependence of intensity $J(\theta)$ for a fixed distance $\xi = 500$ nm and the measured value $\lambda_r(90°) = 400$ nm shows a strong anisotropy of the spin-wave emission pattern characterized by two maxima at $\theta = \pm 90°$ and minima at $\theta = 0°$ and 180° (Fig. 4c), in excellent

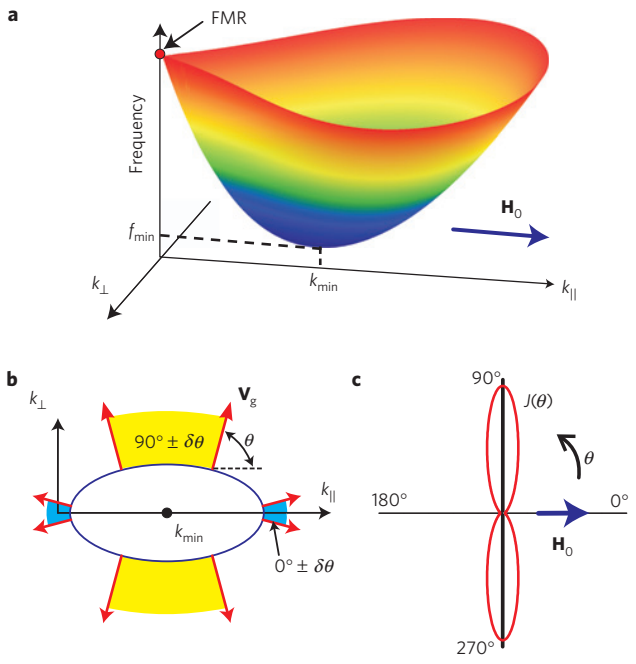

Figure 4 | Analysis of the relationship between the spin-wave spectrum and the spin-wave emission. a, Dependence of the spin-wave frequency f on the wave vector $\mathbf{k} = (k_{\parallel}, k_{\perp})$ oriented at arbitrary direction with respect to the bias field $\mathbf{H}_0$. Points of the dispersion surface characterized by the same frequency are marked by the same colour. FMR: ferromagnetic resonance. **b**, Projection of the contour of constant frequency onto the $(k_{\parallel}, k_{\perp})$ plane. The red arrows show the directions of spin-wave group velocity at different locations on the contour. The light blue and yellow arcs indicate the phase volumes corresponding to the emission of spin waves parallel and perpendicular to $\mathbf{H}_0$, respectively, for the same angular half-intervals $\delta\theta = 15°$. **c**, Angular dependence of spin-wave intensity calculated for $\xi = 500$ nm, $\lambda_r = 400$ nm and the ratio of the effective masses $m_{\parallel}/m_{\perp} = 4$ obtained from the analysis of the spin-wave spectrum.

agreement with the experiment. We emphasize that the presented analysis is valid for any type of quasiparticles with anisotropic effective masses. For example, a similar effect has been observed as focusing of phonons in anisotropic media[27]. One can also expect such effects of directionality in the kinetics of excitons or ballistic electrons injected into a semiconducting film by a local source.

Analysis of the two-dimensional spectrum in Fig. 4a also provides a qualitative explanation for the decrease of the emitted spin-wave intensity at large currents for $\varphi < 45°$ (Fig. 3). Indeed, the strong nonlinear frequency shift at small φ leads to lowering of the generation frequency towards f_{min} and, as a consequence, to a reduction of the group velocity (note that $V_g = 0$ at $f = f_{min}$) and of the decay length λ_r. Smaller λ_r results in a decrease of the spin-wave intensity at the same point of observation. This process represents a gradual two-dimensional version of the predicted nonlinear spin-wave self-localization in STNOs (ref. 15). Nevertheless, our results show that this localization is not complete, and can be avoided by the proper choice of the STNO configuration and the experimental conditions.

We have experimentally demonstrated the operation of STNOs that are characterized by small working currents, do not require large static magnetic fields for their operation and support directional steerable emission of spin waves into the surrounding magnetic film. These features make them the best candidates for realization of nanoscale oscillator arrays. The unexpected finding of strongly directional electronically steerable spin-wave emission is of large importance for new applications of magnetization dynamics in spin-wave logic circuits and spin-wave-based exchange of signals in next-generation integrated digital circuits. Moreover, our analysis indicates that directional emission is a general consequence of anisotropic dispersion, which should be observable in other systems of quasiparticles with anisotropic effective masses. Thus, our findings present us with new and unexpected realities that transcend the field of nanomagnetism, and pave the way for the discovery of new fascinating effects in other physical systems.

Methods

Fabrication. Multilayers Cu(40)Py(6)Cu(3)$Co_{70}Fe_{30}$(9)Au(5) (all thicknesses in nanometres) were sputtered at room temperature on sapphire substrates with electrical leads patterned into coplanar microstrips. An elliptical 100 nm × 50 nm Al(50) mask was defined with a precision of ±5 nm by electron-beam lithography and evaporation. The Au(5) cap, CoFe(9) and Cu(3) were patterned by Ar ion milling through the Al mask, followed by sputtering of a SiO_2(40) insulating layer. To avoid accidental partial patterning of the Py(6) film, the ion-milling rates were pre-calibrated *in situ* by a quartz microbalance. The Al mask was removed by oblique Ar ion milling and etching in KOH solution in H_2O, followed by sputtering of a 1-μm-wide Au(150) top contact. The samples were characterized by atomic force microscopy carried out in semi-contact mode in a Ntegra Aura system (NT-MDT, Russia).

Measurements. The samples were soldered into a holder with optical access for BLS measurements, as well as microstrips for broadband electronic measurements. The sample leads were connected through a bias tee to a current source and a spectrum analyser (HP8563A, Hewlett Packard) via a broadband amplifier. All measurements were carried out at room temperature. The frequency-dependent gain of the amplifier, and the microwave losses in the cables and the sample leads were determined with a calibrated microwave generator and a power meter. The measured microwave signals were corrected for these gains/losses after subtracting the background determined at $I = 0$. Micro-focus BLS measurements were carried out by focusing light produced by a continuous-wave single-frequency laser operating at the wavelength of 532 nm into a diffractionally limited spot. The light scattered from spin waves was analysed by a six-pass Fabry–Perot interferometer TFP-1 (JRS Scientific Instruments) to obtain information about the BLS intensity proportional to the intensity of spin waves at the location of the focal spot. By rastering the probing spot over the surface of the sample using a closed-loop piezo-scanner, two-dimensional maps of the spin-wave intensity were recorded with a resolution of 250 nm. The positioning system was stabilized by custom-designed active feedback, providing long-term spatial stability of better than 50 nm.

Received 21 June 2010; accepted 17 September 2010; published online 24 October 2010

References

1. Myers, E. B., Ralph, D. C., Katine, J. A., Louie, R. N. & Buhrman, R. A. Current-induced switching of domains in magnetic multilayer devices. *Science* **285,** 867–870 (1999).
2. Katine, J. A., Albert, F. J., Buhrman, R. A., Myers, E. B. & Ralph, D. C. Current driven magnetization reversal and spin wave excitations in Co/Cu/Co pillars. *Phys. Rev. Lett.* **84,** 4212–4215 (2000).
3. Tsoi, M. *et al.* Generation and detection of phase-coherent current-driven magnons in magnetic multilayers. *Nature* **406,** 46–48 (2000).
4. Kiselev, S. I. *et al.* Microwave oscillations of a nanomagnet driven by a spin-polarized current. *Nature* **425,** 380–383 (2003).
5. Urazhdin, S., Birge, N. O., Pratt, W. P. Jr & Bass, J. Current-driven magnetic excitations in permalloy-based multilayer nanopillars. *Phys. Rev. Lett.* **91,** 146803 (2003).
6. Rippard, W. H., Pufall, M. R., Kaka, S., Russek, S. E. & Silva, T. J. Direct-current induced dynamics in $Co_{90}Fe_{10}/Ni_{80}Fe_{20}$ point contacts. *Phys. Rev. Lett.* **92,** 27201 (2004).
7. Covington, M., Al Haj Darwish, M., Ding, Y., Gokemeijer, N. J. & Seigler, M. Current-induced magnetization dynamics in current perpendicular to the plane spin valves. *Phys. Rev. B* **69,** 184406 (2004).
8. Krivorotov, I. N. *et al.* Time domain measurements of nanomagnet dynamics driven by spin-transfer torques. *Science* **307,** 228–231 (2005).
9. Mancoff, F. B., Rizzo, N. D., Engel, B. N. & Tehrani, S. Phase-locking in double-point-contact spin-transfer devices. *Nature* **437,** 389–392 (2005).
10. Kaka, S. *et al.* Mutual phase-locking of microwave spin torque nano-oscillators. *Nature* **437,** 389–392 (2005).
11. Pufall, M. R., Rippard, W. H., Russek, S. E., Kaka, S. & Katine, J. A. Electrical measurement of spin-wave interactions of proximate spin transfer nanooscillators. *Phys. Rev. Lett.* **97,** 087206 (2006).
12. Slonczewski, J. C. Current-driven excitation of magnetic multilayers. *J. Magn. Magn. Mater.* **159,** L1–L7 (1996).

13. Berger, L. Emission of spin waves by a magnetic multilayer traversed by a current. *Phys. Rev. B* **54,** 9353–9358 (1996).
14. Slavin, A. Microwave sources: Spin-torque oscillators get in phase. *Nature Nanotechnol.* **4,** 479–480 (2009).
15. Slavin, A. & Tiberkevich, V. Spin wave mode excited by spin-polarized current in a magnetic nanocontact is a standing self-localized wave bullet. *Phys. Rev. Lett.* **95,** 237201 (2005).
16. Hoefer, M. A., Ablowitz, M. J., Ilan, B., Pufall, M. R. & Silva, T. J. Theory of magnetodynamics induced by spin torque in perpendicularly magnetized thin films. *Phys. Rev. Lett.* **95,** 267206 (2005).
17. Consolo, G. *et al.* Micromagnetic study of the above-threshold generation regime in a spin-torque oscillator based on a magnetic nanocontact magnetized at an arbitrary angle. *Phys. Rev. B* **78,** 014420 (2008).
18. Hoefer, M. A., Silva, T. J. & Stiles, M. D. Model for a collimated spin-wave beam generated by a single-layer spin torque nanocontact. *Phys. Rev. B* **77,** 144401 (2008).
19. Chen, X. & Victora, R. H. Phase locking of spin-torque oscillators by spin-wave interactions. *Phys. Rev. B* **79,** 180402(R) (2009).
20. Berkov, D. V. & Gorn, N. L. Spin-torque driven magnetization dynamics in a nanocontact setup for low external fields: Numerical simulation study. *Phys. Rev. B* **80,** 064409 (2009).
21. Demidov, V. E., Demokritov, S. O., Hillebrands, B., Laufenberg, M. & Freitas, P. P. Radiation of spin waves by a single micrometre-sized magnetic element. *Appl. Phys. Lett.* **85,** 2866–2868 (2004).
22. Demokritov, S. O. & Demidov, V. E. Micro-Brillouin light scattering spectroscopy of magnetic nanostructures. *IEEE Trans. Magn.* **44,** 6–12 (2008).
23. Demidov, V. E. *et al.* Magnon kinetics and Bose–Einstein condensation studied in phase space. *Phys. Rev. Lett.* **101,** 257201 (2008).
24. Kalinikos, B. A. Excitation of propagating spin waves in ferromagnetic films. *IEE Proc. H* **127,** 4 (1980).
25. Kalinikos, B. A. & Slavin, A. N. Theory of dipole-exchange spin-wave spectrum for ferromagnetic films with mixed exchange boundary conditions. *J. Phys. C* **19,** 7013 (1986).
26. Ascroft, N. W. & Mermin, N. D. *Solid State Physics* Ch. 12 (Saunders College, 1976).
27. Northrop, G. A. & Wolfe, J. P. Ballistic phonon imaging in germanium. *Phys. Rev. B* **22,** 6196–6212 (1980).

Acknowledgements

We acknowledge support from Deutsche Forschungsgemeinschaft, the European Project Master (No. NMP-FP7 212257), NSF, the Research Corporation and the WVNano initiative.

Author contributions

V.E.D. carried out measurements and data analysis, S.U. fabricated the samples and S.O.D. formulated the experimental approach and designed the measurement instrumentation. All authors co-wrote the manuscript.

Additional information

The authors declare no competing financial interests. Reprints and permissions information is available online at http://npg.nature.com/reprintsandpermissions. Correspondence and requests for materials should be addressed to V.E.D.